ACS OMEGA

http://pubs.acs.org/journal/acsodf

Article

Magnesium Oxide Nanoparticles: Effective Antilarvicidal and Antibacterial Agents

Abinaya S and Helen P. Kavitha*

Cite This: *ACS Omega* 2023, 8, 5225−5233

Read Online

ACCESS | Metrics & More | Article Recommendations

ABSTRACT: People are vulnerable to mosquito-borne infections in tropical and subtropical climate countries. Due to resistive issues, vector control is an immediate concern in today's environment. The current study describes the synthesis of magnesium oxide by four different approaches including green, microwave, sol−gel, and hydrothermal methods. The synthesized magnesium oxide (MgO) nanoparticles were characterized using Fourier transform infrared spectroscopy (FT-IR), X-ray diffraction (XRD), high-resolution scanning electron microscopy (HRSEM), and energy-dispersive X-ray analysis (EDAX) techniques. The FT-IR studies reveal the presence of functional groups in the synthesized nanoparticles. The structural and morphological studies were investigated using XRD and HRSEM. EDAX reveals the presence of Mg and O in the prepared samples. The synthesized MgO NPs were screened for antibacterial studies against Gram-positive strains, *Enterococcus faecalis* and *Staphylococcus aureus*, two Gram-negative cultures, *Escherichia coli* and *Klebsiella pneumoniae*, using different concentrations. The results indicated excellent antibacterial activity against both Gram-positive and Gram-negative bacteria at 50 mg/mL hydrothermally produced MgO nanoparticles, with a maximal zone of inhibition (ZOI) of 5 mm for *S. aureus*, 7 mm for *E. faecalis*, and 6 mm for *K. pneumoniae*. The ZOI of *E. coli* was found to be the greatest at 9 mm when 50 mg/mL sol−gel-produced MgO nanoparticles were used. The synthesized MgO nanostructures were tested against fourth-instar larvae of *Aedes aegypti* and *Aedes albopictus*, and the hydrothermally synthesized MgO nanostructures exhibited better results when compared with other methods of synthesis. The reports show that *A. aegypti* and *A. albopictus* mortality rates were reported to be the lowest with green-manufactured MgO nanoparticles (7.5 g mL^{-1}) and the highest with hydrothermally synthesized MgO nanoparticles (120 g mL^{-1}). The research indicates that MgO nanostructures are promising drugs for antibacterial and mosquitocidal larvae control properties.

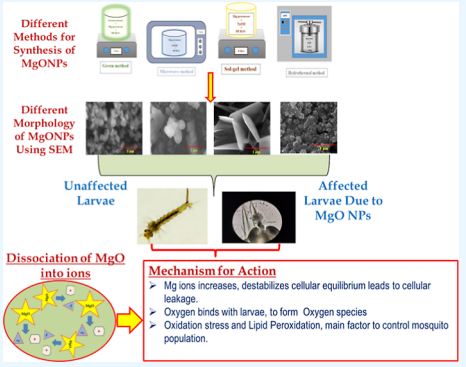

INTRODUCTION

Vector-borne diseases like malaria, dengue fever, yellow fever, and filariasis are considered as massive health concerns. Mosquito species from the genera *Aedes albopictus*, *Aedes stephensi*, and *Culex quinquefasciatus* perform crucial roles in vector-borne disease transmission.[1] Over 2.5 billion people are at high risk of getting infected by dengue virus outbreaks, and an estimated 3.97 billion dengue infections occur each year in about 128 countries, predominantly in tropical and subtropical zones. In India, more than 31,117 persons were affected from dengue fever in 2017.[2] Dengue and chikungunya as well as viruses and other illnesses are spread by the *Aedes aegypti* and *A. albopictus* vector.[3] In addition, because of periodic weather fluctuations, increase in spontaneous urbanization, and world-wide migrations, another viral disease known as dengue fever has spread around the world, causing mortality in many countries.

These species may be spotted in large numbers across several tropical places of the world, and they reproduce quickly in drains and stagnant water reservoirs. Though the usage of synthetic pesticides could stop disease transmission, prolonged usage of pesticides can quickly degrade the ecology and contribute to a mosquito population recovery.[4,5] Also, many people are affected by cough, diarrhoea, skin allergy, and gastric problems due to the usage of synthetic pesticides. Furthermore, a variety of critical clinical methods to heal an infected person from pesticides have been documented.[6]

The implementation of mosquito vector control programs at an earlier stage is better appropriate for mitigating such spread of vector-borne illnesses.[7] Due to their limited motility in breeding sites, targeting the larvae is seen to be a successful technique. Researchers have been looking for an environmentally safe, sustainable, and cost-effective replacement for conventional pesticides to control the abundance of numerous

Received: March 10, 2022
Accepted: December 14, 2022
Published: February 2, 2023

ACS Publications

© 2023 The Authors. Published by American Chemical Society

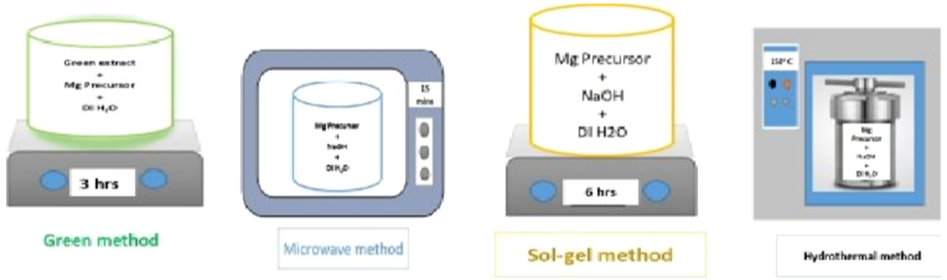

Figure 1. Various methods of synthesis of NPs utilized in this study.

mosquito disease vectors for decades.[8,9] Targeting the larvae is thought to be the most recent potential technology for achieving that aim, with a variety of advantages such as enhanced bioefficacy, longevity, and targeted distribution to particular locations. The introduction of effective nanostructures with better physicochemical characteristics can aid in reducing major environmental problems associated with larvicidal drugs.[10−14] Nanoparticles (NPs) can be synthesized using various techniques such as biological, chemical, and physical methods. This study involves the fabrication of nanostructures by utilizing the above mentioned methods, that is, the biological method includes the usage of green extracts, the chemical method utilizes chemicals, and the physical method involves using external energy like radiation for metal ion reduction. According to literature survey, Au, Ag, and Cd metal nanostructures and oxides of Zn, Mg, Ti, Al, Cu, and Ce can be effectively used as larvicides. Due to their low toxicity and cost-effectiveness, researchers have been working on magnesium oxide nanostructures (magnesium oxide nanoparticles (MgO NPs)].[15] They possess specific importance in the modern field of nanotechnology due to their specific characteristics, which enable them to be used in a variety of applications.[16−18] Because of their low toxicity, MgO NPs have been identified for their potential application in physiological systems.[19]

Magnesium are abundant in the earth's crust and have more availability than other metals. The motive of the research is to extensively develop innovative nanosized MgO materials which are synthesized in four different ways (Figure 1). The first method is green nanosynthesis[20] which is economical and environmentally friendly and focused on ensuring the total removal of potentially harmful waste materials. Also, this method utilizes minimum chemicals for nanoparticle synthesis. Second, we focused on the microwave irradiation method[21] which is one of the most promising techniques available today. This technique is simple to use and allows for rapid heating, easy size control, and formation of fewer products. The interaction of the molecule's permanent dipole moment with high-frequency electromagnetic radiation produces the heating effect. Any material's ability to absorb microwave energy is represented by its dielectric loss factor multiplied by the dielectric constant.[22] The third method for the MgO synthesis is the sol−gel method,[23] which is also one of the promising techniques for the synthesis of nanostructures. It is simple, economical, and operable even at low temperatures. Finally, the hydrothermal method is employed for the synthesis of MgO nanostructures which can produce crystalline phases. Few distinct species of mosquito vectors have been studied extensively using MgO nanostructures.

Thus-synthesized nanostructures are examined using various characterization techniques. In addition, antibacterial and larvicidal activities were also studied.

MATERIALS AND METHODS

Materials. Magnesium nitrate hexahydrate [$Mg(NO_3)_2 \cdot 6H_2O$] and sodium hydroxide (NaOH) were purchased from Merck. All of the other chemicals and reagents used in this experiment were of analytical grade quality. *Psidium guajuava* leaves were collected from Tamil Nadu, India, in October.

Methods. *Green Synthesis (G-MgO).* Freshly picked *P. guajuava* leaves were collected, washed under running water, and dried under dark condition for 5 to 6 days. Then, the leaves were powdered using a blender. About 10 g of the obtained powdered leaves were added to water, heated at 50 °C, and stirred for 30 min. Then, the solution was cooled to room temperature, filtered, and stored at 4 °C until further use.

0.1 mM (1.8 g) magnesium nitrate hexahydrate was dissolved in 100 mL of deionized water and stirred for 15 min. To the prepared solution, 15 mL of *P. guajuava* leaf extract was added and stirred using a magnetic stirrer for 3 h resulting in the formation of a brownish yellow solution which is evidence for the generation of magnesium hydroxide nanoparticles (MgH NPs). The obtained suspension was washed with water and ethanol to remove the impurities present in the solution. Then, the washed solution was centrifuged at 4000 rpm for 10 min and calcined at 400 °C for 4 h to obtain the pure form of MgO NPs. Without the addition of any external agents (like NaOH), the leaf extract itself acts as both reducing and capping agents.

Microwave Synthesis Method (M-MgO). MgO NPs were synthesized using the microwave synthesis method. 0.1 mM (1.8 g) magnesium nitrate hexahydrate was dissolved in 100 mL of deionized water and stirred for 30 min. After that, 0.1 M NaOH was added into the magnesium precursor solution. Instantly, a white suspension was formed which confirms the formation of MgH NPs. This suspension was further allowed for irradiation with microwaves in a microwave furnace for about 15 min. Then, the obtained MgO NPs were washed with water and ethanol to remove the impurities present in the solution. Then, the washed solution was centrifuged at 4000 rpm for 10 min and calcined at 400 °C for 4 h to get MgO NPs.

Sol−Gel Synthesis Method (SG-MgO). The process of synthesis of MgO NPs involves dissolving 0.1 mM (1.8 g) magnesium nitrate hexahydrate in 100 mL of deionized water to get the precursor solution to which 0.1 M NaOH solution was added. White suspended particles were formed which clearly shows the formation of MgH NPs. Then, the solution was stirred for 6 h and washed with water and ethanol until the

https://doi.org/10.1021/acsomega.2c01450
ACS Omega 2023, 8, 5225−5233

pH reached 7. Then, the washed solution was centrifuged at 4000 rpm for 10 min and calcined at 400 °C for 4 h.

Hydrothermal Synthesis (HY-MgO). MgO nanostructures were synthesized using hydrothermal method by dissolving 0.1 mM (1.8 g) Mg precursor solution in 100 mL of deionized water to which 0.1 M NaOH was added. White suspended particles were formed which confirms the formation of MgH NPs. The resultant solution was stirred using a magnetic stirrer for about 60 min, and then the solution was transferred into a Teflon-lined stainless steel autoclave and maintained at 150 °C for 24 h. Then, the solution was washed with water and ethanol until the pH reached 7. Then, the washed solution was centrifuged at 4000 rpm for 10 min and calcined at 400 °C for 4 h.

Characterization Techniques. The presence of organic moieties in the synthesized MgO NPs was studied using a PerkinElmer Fourier transform infrared (FT-IR) spectrometer with the wavelength from 400 to 4000 cm^{-1}. X-ray diffractometer (XRD) pattern was observed using a BRUKER USA D8 Advance, Davinci powder X-ray diffractometer using CuK_{α} radiation with the wavelength (λ) of 1.5406 Å. The surface morphology of the synthesized MgO NPs was studied using high resolution-scanning electron microscopy (HRSEM, Thermo Sceintific Apreo S).

Antibacterial Assay. Using the well diffusion method, the antibacterial activities of the synthesized MgO NPs were analyzed against both Gram-positive and Gram-negative bacterial isolates given in Table 1.

Table 1. Bacterial Strains Used for Antibacterial Analysis Activity

s. no	type of bacteria	name of the bacteria	culture collection
1.	Gram Positive	S. aureus	ATCC 6538
2.	Gram Positive	E. faecalis	ATCC 9027
3.	Gram Negative	E. coli	ATCC 8739
4.	Gram Negative	K. pneumoniae	ATCC 13883

The bacterial strains were grown on Muller–Hinton broth at 35 °C on a rotary shaker at 200 rpm. Using sterile cotton swabs, each and every culture was individually coated uniformly on the Petri dishes in which five wells of 6 mm diameter were created using gel puncture on each Muller–Hinton plate. In the prepared wells, about mg/mL ampicillin and various concentrations of 10, 20, 30, and 50 mg/mL MgO NPs (G-MgO, M-MgO, SG-MgO, and HY-MgO) were introduced and incubated at 35 °C for 24 h.[24] Then, the zone of inhibition (ZOI) were evaluated after the process of incubation.

Insect Rearing Techniques. Larvae were gathered from a stagnant water in Chennai and identified in the King Institute of Preventive Medicine, Guindy, Chennai, India. *A. aegypti* and *A. albopictus* early fourth-instar larvae were obtained regionally and housed in plastic containers with dechlorinated tap water. They were preserved as stated earlier.[14]

Larvicidal Assay. The larvicidal activities were evaluated[25] with minor alteration, as reported by Rahuman et al. (2000).[26] The preparation of the stock solution involves adding 1 mL of MgO nanostructures to 100 mL of double-distilled water. For performing the bioassay test of the MgO NPs, 120 ppm solution was taken from the above prepared stock and added to the dechlorinated water.

The toxicity of synthesized MgO was studied by preparing stock solution in 120, 60, 30, 15, and 7.5 ppm concentrations. About 20 mosquito larvae was placed into 200 mL of double-distilled water. Each experiment contained a control group (distilled water) and five replicates of each concentration of MgO nanostructures. Acute toxicity of fourth-instar larvae of *A. aegypti* and *A. albopictus* was studied by measuring the mortality rate after 24 h.

Dose–Response Bioassay. Depending on the early screening results, the prepared NPs were tested against *A. aegypti* and *A. albopictus* larvae in a dose-response bioassay. For larvicidal action, several concentrations ranging from 120, 60, 30, 15, and 7.5 ppm (prepared NPs) were produced. After 24 h of exposure, the number of dead larvae was counted, and the mortality percentage was calculated using the average of five replicates.

Statistical Analysis. The average larvae mortality rate was subjected to probit analysis to determine LC_{50} and LC_{90} values by using SPSS (version 16.0) software. The values were expressed in terms of (SD $\pm$ n = 3) replicates.

RESULTS AND DISCUSSION

MgO nanostructures were synthesized using various methods like Green synthesis, microwave synthesis, sol–gel synthesis,

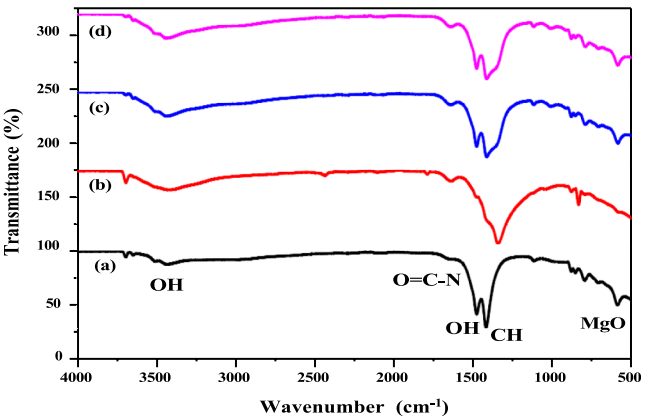

Figure 2. FT-IR image of (bottom to top) green (a), microwave (b), sol–gel (c), and hydrothermal methods (d) of preparation of MgO nanostructures.

and hydrothermal synthesis. FT-IR studies were performed to study the probable biomolecules or chemicals which are responsible for the capping and effective stability of MgO NPs.

The FT-IR chromatogram observed from the synthesized MgO NPs is shown in Figure 2. In Figure 2, the broad peak at 3420 cm^{-1} corresponds to antisymmetric stretching vibration arising from –OH groups. The FT-IR image of green-synthesized MgO NPs represented in graph 2a consists of a broad peak at 3420 cm^{-1} which is due to the presence of polyphenols within the *P. guajuava* leaf extract used in the process of synthesis of MgO NPs. The micrographs 2b (microwave), 2c (sol–gel), and 2d (hydrothermal) also have a broad peak at 3420 cm^{-1} which is also formed due to the presence of OH molecule that is responsible for the formation of MgO NPs from its precursor and also due to the N–H bending of the amine bond.[27] The medium peak observed at 1630 cm^{-1} corresponds to the bending mode of the primary amine (N–H) overlapped with either amide or carboxylate salt.[28] The band at 1647 cm^{-1} is a result of the amide group

https://doi.org/10.1021/acsomega.2c01450
ACS Omega 2023, 8, 5225–5233

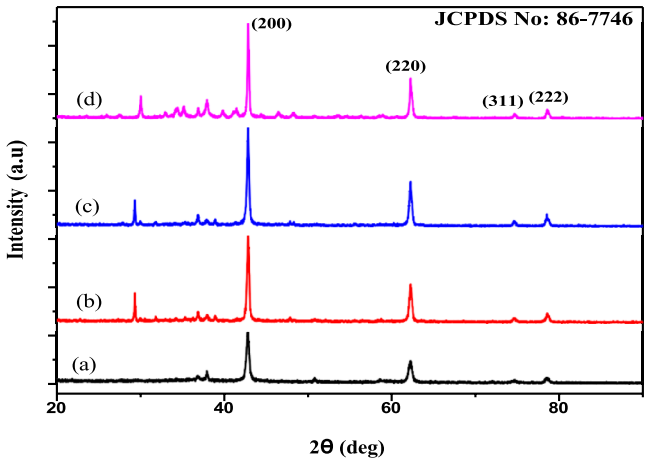

Figure 3. X-ray powder diffraction pattern of (bottom to top) green (a), microwave (b), sol−gel (c), and hydrothermal (d) methods of preparation of MgO nanostructures.

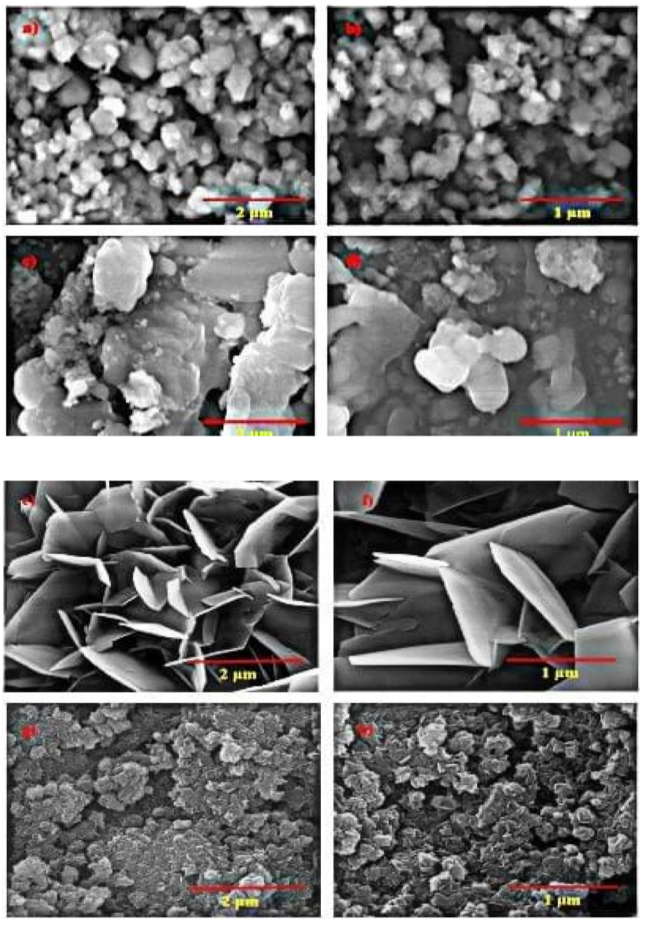

Figure 4. SEM micrographs of (top to bottom) green (a,b), microwave (c,d), sol−gel (e,f), and hydrothermal (g,h) methods of preparation of MgO nanostructures.

(O═C−NH).[29] The presence of a peak at 1484 cm^{-1} is due to the vibrations of the carbonate ion (C−O).[30] The peaks at 1420 and 1413 cm^{-1} show the presence of OH within the compound. The most intense band (M) at 1351 cm^{-1} is related to the C−H bending vibrations of the aliphatic group.[31] The peaks that appear between the wave number 400 and 700 cm^{-1} confirm the presence of MgO at the nanoscale.[32−34] The peaks observed in FT-IR spectra manifest the purity of the synthesized NPs and confirms the presence of Mg−O at the nanoscale.

The crystallographic structure of different methods of synthesized MgO NPs was studied using XRD analysis. XRD spectra (Figure 3) showed major intense peaks at 2θ values of 42.68, 62.4, 74.28, and 78.62° corresponding to (200), (220), (311), and (222). The obtained diffraction peaks matched well with the crystallographic structure according to JCPDS standard (JCPDS file no. 89-7746).[28,35] According to XRD spectra, the presence of Mg $(OH)_2$ and MgO in the synthesized samples obtained by various methods is confirmed. The observed peaks at 2θ of 29.81, 75.08, and 78.64° corresponded to $Mg(OH)_2$. The average crystalline size can be calculated according to XRD analysis using the Debye−Scherrer equation, which was found to be 29.5 nm for HY-MgO, 33.8 nm for sol−gel synthesized MgO nanostructures, 49.5 nm for microwave-assisted MgO nanostructures, and 44.7 nm for green-synthesized MgO nanostructures.

The surface morphology of the synthesized MgO nanostructures was examined using HRSEM micrographs as shown in Figure 4. The XRD micrographs show the highest intensity peaks and crystallite nature and that can be clearly found from the SEM images especially in hydrothermally synthesized MgO NPs. The green-synthesized MgO NPs are shown in Figure 4a,b which exhibit uniform spherical-shaped MgO NPs with the size 85.8 nm. Microwave-synthesized MgO NPs (4c and 4d) exhibit an irregular spherical pattern with a particle size of 100 nm. The SEM topographs of sol−gel-synthesized MgO NPs showed the formation of uniform platelike structures with 70 nm size (4e and 4f). The panoramic morphology of the hydrothermally synthesized MgO NPs consist of flowerlike morphology having 60 nm particle size. Cautious examination found that the NPs consist of a disclike morphology. Also, these micrographs exhibited dense, porous, and agglomerated structures. From the obtained SEM micrographs, it is evident that the different methods of MgO NP synthesis show different morphologies which is due to the surface energy and size. Also, Figure 5A−D shows the presence of Mg and O ions in the samples, which was confirmed by the energy-dispersive X-ray analysis (EDAX) profile.

The antibacterial activity of MgO nanostructures has been examined employing a variety of analytical approaches. The antibacterial study reveals that the hydrothermal-assisted MgO nanostructures exhibited excellent antibacterial activity when compared with all other methods, and the ZOI was carried out by measuring the observed inhibition on the well by the diffusion method shown in Table 2. The HY-MgO NPs produced a potent ZOI in the respective well of 50 mg/mL and showed a maximum ZOI of 3 mm for *Staphylococcus aureus*, 7 mm for *Enterococcus faecalis*, 5 mm for *Escherichia coli*, and 6 mm for *Klebsiella pneumoniae*. The results (ZOI) obtained from the other MgO NPs are very less when compared with the HY-MgO NPs (Figure 6).

The antibacterial effect of MgO nanostructures has been proved to be size-dependent in numerous studies. According to Huang et al. (2005),[36] a decrease in the particle size of MgO boosted the antibacterial activity. The bactericidal efficacy of nano-MgO increased slowly with the decrease in the particle size for particles in the size range of 29.5 to 49.5 nm. Makhluf et al. (2005)[19] found that nanoscale MgO nanostructures were effective against Gram-positive and Gram-negative bacteria. The findings demonstrated a definite size effect, with the

https://doi.org/10.1021/acsomega.2c01450
ACS Omega 2023, 8, 5225−5233

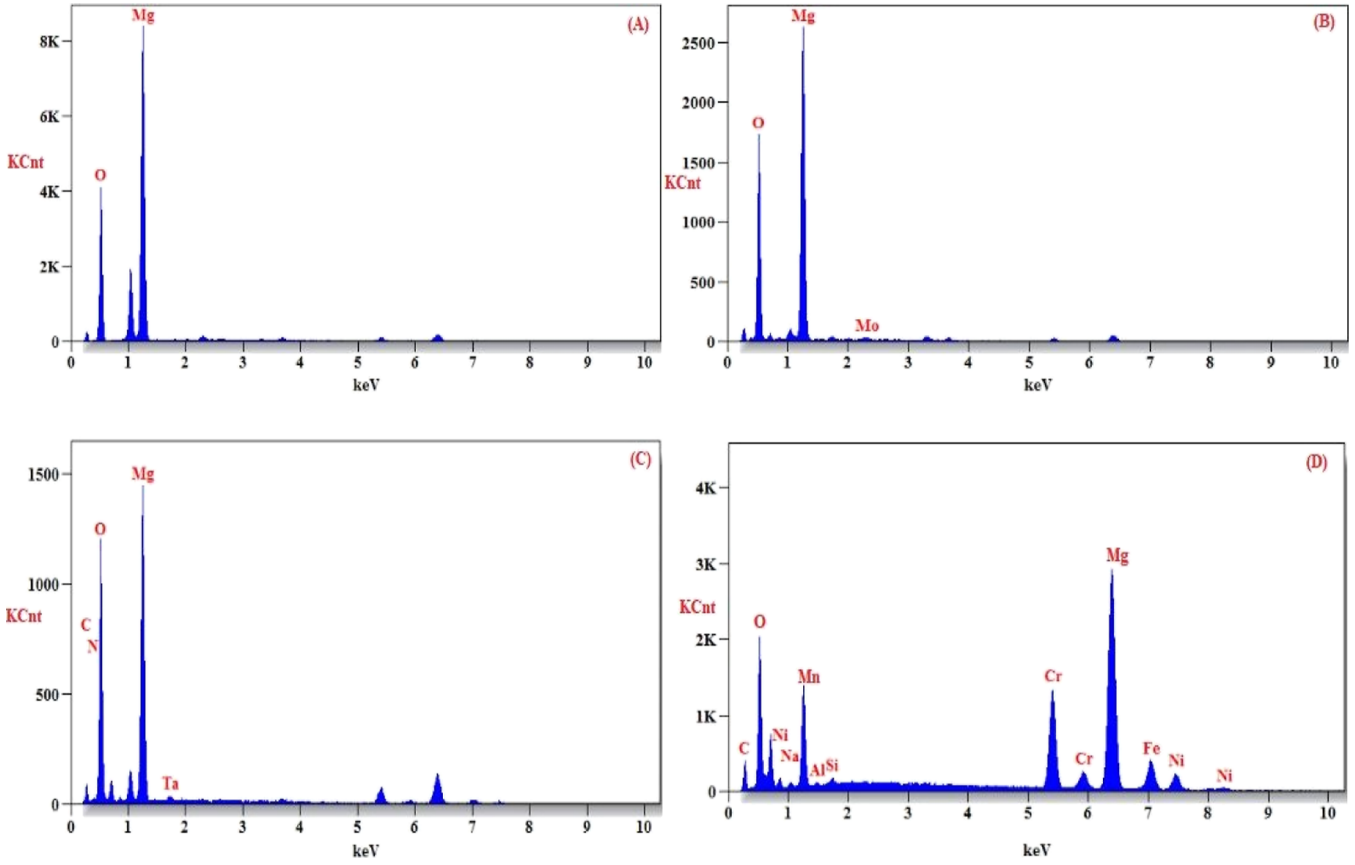

Figure 5. (A–D) EDAX micrographs of green (A), microwave (B), sol–gel (C), and hydrothermal (D) methods of preparation of MgO nanostructures.

Table 2. Zone of Inhibition of G-, M-, S-, and H-MgO NPs Activity Against *S. aureus*, *E. faecalis*, *E. coli*, and *K. pneumoniae* (A: Antibiotic Used)[a]

		ZOI (mm)																			
		green synthesis (mg/mL)					microwave synthesis (mg/mL)					sol–gel synthesis (mg/mL)					hydrothermal synthesis (mg/mL)				
s. no	name of pathogens	A	10	20	30	50	A	10	20	30	50	A	10	20	30	50	A	10	20	30	50
1.	S. aureus	6	0.4	0	1	2.4	4	0	0	0.5	2.2	10	0	0	0	0	10.4	1	1.5	2	5
2.	E. faecalis	3	0	0	1	2	10	0	0	1.4	5.3	10.2	0	0	0	1	10.8	3	4	5	7
3.	E. coli	10	0	1	1	3	10.2	0	0	0	1	10.5	0	0	2	9	10.1	2	2	3	5
4.	K. pneumoniae	11.2	0	0	1	1.3	1	0	0	0	2	10.3	0	0	0.3	1	10.2	4	3	4	6

[a]Values represent mean ± SD of three replicates. Statistically significant at $p < 0.05$.

number of microorganisms destroyed being strongly influenced by the particle size. As the size of MgO nanostructures decreases, the specific surface area of the nanostructures increases. Hence, it is evident that MgO nanostructures synthesized using the hydrothermal method (29.5 nm) shows a small particle size when compared with the other methods. The potential number of reactive groups on the particle surface, which are believed to have significant antibacterial activity, is determined by the increase in surface area.[37,38] Also, as per Jin and He (2011),[39] higher MgO NP concentrations resulted in more bacterial inactivation.

The actual mechanism of inhibiting the bacterial growth using MgO nanostructures is still mysterious. A number of processes have been proposed to explain the antibacterial mechanism of MgO nanostructures, including the generation of reactive oxygen species (ROS), the interaction of nanostructures with bacteria, resulting in bacterial cell damage, and an alkaline response. Antibacterial mechanisms also comprise the activation of oxidative stress as a result of the production of ROS, which can lead to distortion of the cell membrane structure.[40,41] Many research studies have suggested that MgO nanostructure antibacterial action is due to the formation of ROS, such as superoxide anion (O^{2-}).[42−44] It has been disclosed that when the surface area of the MgO NPs increases, the concentration of O^{2-} in the solution also increases which ultimately leads to cell death. Also, it has been proved that the interaction could be caused by an electrostatic interaction between positively charged MgNPs and the negatively charged cell wall membrane.[45]

Traditional approaches (either biological or chemical) have been widely used for limiting the spread of mosquitoes. However, these methods have downsides, such as toxicity to consumers and a rise in mosquito resistance to these substances.[46] Because of their distinct properties, NPs have

https://doi.org/10.1021/acsomega.2c01450
ACS Omega 2023, 8, 5225−5233

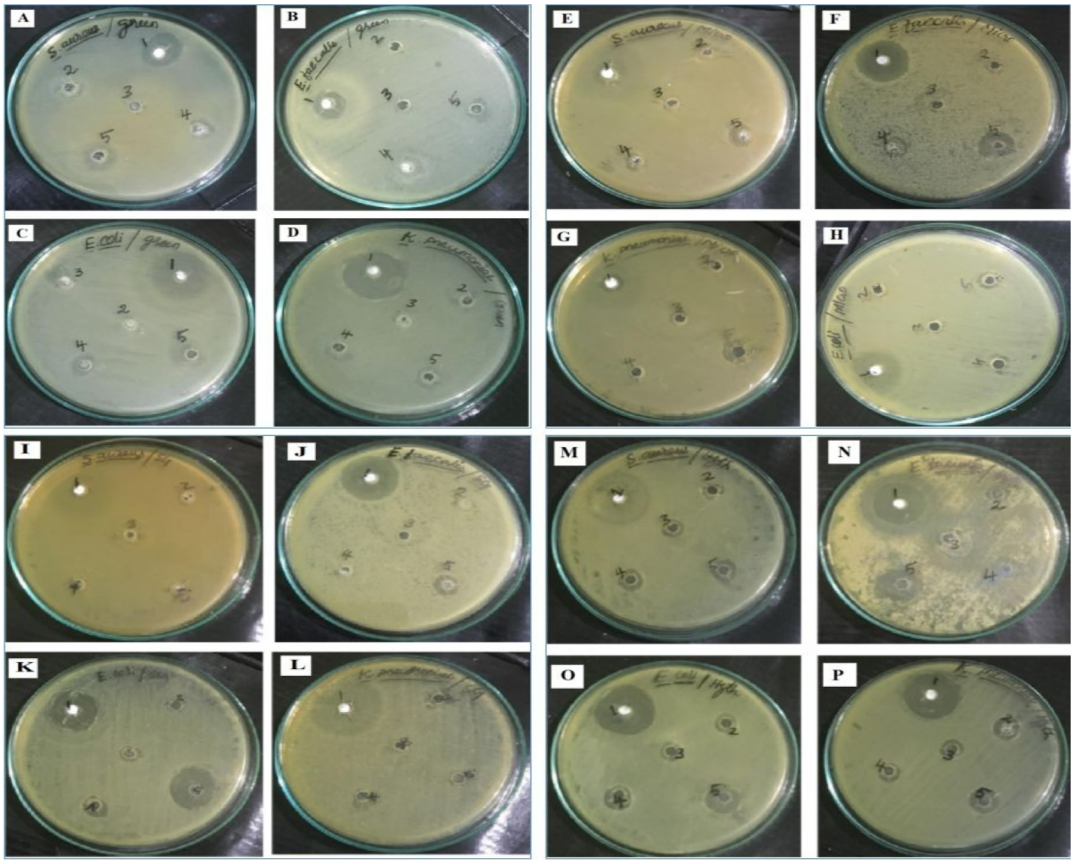

Figure 6. ZOI of green (A−D), microwave (E−H), sol−gel (I−L), and hydrothermal (M−P) synthesized MgO NPs activity against *S. aureus*, *E. faecalis*, *E. coli*, and *K. pneumoniae*.

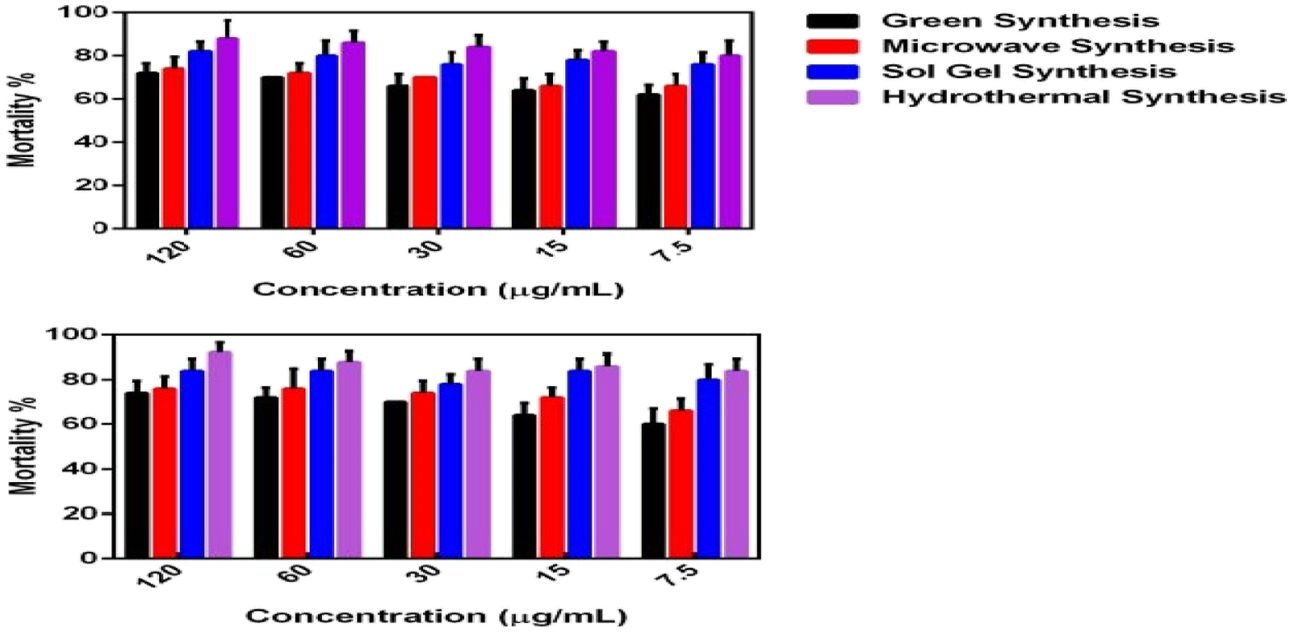

Figure 7. Mortality rate of *A. albopictus* and *A. aegypti* against various concentrations of MgO NPs.

recently been employed as a replacement to traditional approaches for controlling mosquito-borne infections.[47−49] The mortality rate of the larvae depends on the concentration of MgO NPs. The mortality rates of *A. aegypti* and *A. albopictus* are given in Figure 7 which evidently shows that the lowest death percentage (60%) was acquired with green-synthesized 7.5 μg mL^{-1} MgO NPs, while the highest mortality percentage (96%) was found with hydrothermally synthesized 120 μg mL^{-1} MgO NPs. It is interesting that hydrothermally produced MgO NPs show excellent activity against *A. aegypti* and *A. albopictus* when compared with the other methods. Since the nanostructures are known to have a smaller size (29.5 nm) and

https://doi.org/10.1021/acsomega.2c01450
ACS Omega 2023, 8, 5225−5233

Table 3. Larvicidal Activity of Green-Synthesized MgO NPs Against *A. aegypti* (I) and *A. albopictus* (II) Larvae[a]

		green synthesis (mg/mL)						microwave synthesis (mg/mL)						sol−gel synthesis (mg/mL)						hydrothermal synthesis (mg/mL)					
		mortality		LC_{50}		LC_{90}		mortality		LC_{50}		LC_{90}		mortality		LC_{50}		LC_{90}		mortality		LC_{50}		LC_{90}	
s. no	concentration	I	II	I	II	I	II	I	II	I	II	I	II	I	II	I	II	I	II	I	II	I	II	I	II
1.	50	74	76	14	20	28	39	76	74	27	25	47	49	84	82	33	39	47	71	92	88	33	50	61	92
2.	25	72	76					76	72					84	80					88	86				
3.	12.5	70	74					74	70					78	76					84	84				
4.	6.25	64	72					72	66					84	78					86	82				
5.	3.125	60	66					66	66					80	76					84	80				

[a]Values represents mean ± SD of three replicates. Statistically significant at $p < 0.05$.

a larger surface area, it is extremely beneficial for biomedical applications. It is obvious from field emission SEM (FESEM) that the smaller-sized hydrothermally synthesized MgO NPs perform better toward the pathogenic bacterial strains. MgO NPs may affix on the surface of the mosquito respiratory tracts due to their reduced size, causing asphyxia and cell death. The enhanced activity by the hydrothermal synthesis MgO NPs might be due to the crystalline nature and platelike structure which is evident from the XRD and FESEM analyses. Table 3 projects the LC_{50} (concentration of MgO NPs that inhibit 50% of the population) and LC_{90} (concentration of MgO NPs that inhibit 90% of the population) values from all synthesis methods. The study shows that when the concentration of the NPs decreases, the mortality rate is also decreased, and both the factors are directly proportional to each other. The generation of ROS and lipid peroxidation, as well as the leakage of internal cellular contents due to cell membrane disruption, may be involved in the mosquitocidal mechanism of MgO NPs.[50,51] MgO NPs are decomposed into Mg^{2+} and O^{2-} ions in the surrounding environment after being sprayed over one stage of the mosquito life cycle, such as the egg, larvae, pupa, or adult. The elevated level of O^{2-} ions produces ROS,[52] which causes oxidative stress and lipid peroxidation. Furthermore, because of their small size, MgO NPs can react with nucleic acid which distorts and restricts the mosquito proliferation.[53] However, a high concentration of Mg^{2+} can cause the cellular equilibrium to be disrupted or damaged, resulting in increased stress, cellular component leakage, and ultimately cell death.[54] The current study focuses on the mortality rate of the mosquito larvae *A. aegypti* and *A. albopictus*.

CONCLUSIONS

The MgO nanostructures have been successfully synthesized using four different approaches. Thus-synthesized MgO nanostructures have been characterized using XRD, FT-IR, and SEM-EDAX techniques. Hydrothermal-synthesized MgO NPs show excellent morphology with 29.5 nm particle size. The SEM micrographs exhibited a uniform spherical shape for green-synthesized NPs, an irregular spherical pattern for microwave-synthesized NPs, a uniform plate-like structure for sol−gel-synthesized NPs, and a flowerlike morphology for hydrothermally synthesized NPs. The antibacterial activity was studied against the pathogenic bacterial strains such as *S. aureus*, *E. faecalis*, *E. coli*, and *K. pneumoniae*. Also, the data showed that the inhibitory activity of MgO NPs is concentration-dependent. The data analysis report shows that 50 mg/mL hydrothermally produced MgO NPs have a good antibacterial activity, with a maximal ZOI of 5 mm for *S. aureus*, 7 mm for *E. faecalis*, and 6 mm for *K. pneumoniae*. The ZOI of *E. coli* was found to be maximum at 9 mm with 50 mg/mL sol−gel-synthesized MgO NPs. Also, the mortality rates of *A. aegypti* and *A. albopictus* were found to be the lowest with green-synthesized MgO NPs (7.5 $\mu g\ mL^{-1}$) and the highest with hydrothermally synthesized MgO NPs (120 $\mu g\ mL^{-1}$).

AUTHOR INFORMATION

Corresponding Author

Helen P. Kavitha − *SRM Institute of Science and Technology, Chennai 600089, India;* orcid.org/0000-0002-9099-7937; Email: helenkavithap2020@gmail.com

https://doi.org/10.1021/acsomega.2c01450
ACS Omega 2023, 8, 5225−5233

Author

Abinaya S − *SRM Institute of Science and Technology, Chennai 600089, India*

Complete contact information is available at: https://pubs.acs.org/10.1021/acsomega.2c01450

Notes

The authors declare no competing financial interest.

■ ACKNOWLEDGMENTS

The authors would like to thank the support from the SRM Institute of science and technology, Ramapuram campus, Chennai, India for permitting to perform research work and providing lab facilities. The authors express their greatest gratitude to the SCIF—SRM Institute of science and technology, Kattankulathur for helping us analyzing the samples. No funds have been raised.

■ REFERENCES

(1) Mittal, P. K.; Subbarao, S. K. Prospects of using herbal products in the control of mosquito vectors. *ICMR Bull.* **2003**, *33*, 1−10.

(2) *National Vector Borne Disease Control Programme*; Directorate General of Health Services, 2017.

(3) *Filariasis, in Ciba Foundation Symposium*; Mak, J. W., Evered, D., Clark, S., Eds.; John Wiley & Sons: Chichester, UK, 2007; Vol. *127*.

(4) Mathivanan, T.; Govindarajan, M.; Elumalai, K.; Krishnappa, K.; Ananthan, A. Mosquito larvicidal and phytochemical properties of Ervatamia coronaria Stapf. (Family: Apocynaceae). *J. Vector Borne Dis.* **2010**, *47*, 178−180.

(5) Tiwary, M.; Naik, S. N.; Tewary, D. K.; Mittal, P. K.; Yadav, S. Chemical composition and larvicidal activities of the essential oil of *Zanthoxylum armatum* DC (Rutaceae) against three mosquito vectors. *J. Vector Borne Dis.* **2007**, *44*, 198.

(6) Cohen, J. M.; Smith, D. L.; Cotter, C.; Ward, A.; Yamey, G.; Sabot, O. J.; Moonen, B. Malaria resurgence: a systematic review and assessment of its causes. *Malar. J.* **2012**, *11*, 1−17.

(7) Howard, A. F.; Zhou, G.; Omlin, F. X. Malaria mosquito control using edible fish in western Kenya: preliminary findings of a controlled study. *BMC Public Health* **2007**, *7*, 199.

(8) Al-Mehmadi, R. M.; Al-Khalaf, A. A. Larvicidal and histological effects of Melia azedarach extract on Culex quinquefasciatus Say larvae (Diptera: Culicidae). *J. King Saud Univ., Sci.* **20102010**, *22*, 77−85.

(9) Kamaraj, C.; Abdul Rahman, A.; Bagavan, A.; Abduz Zahir, A.; Elango, G.; Kandan, P.; Rajakumar, G.; Marimuthu, S.; Santhoshkumar, T. Larvicidal efficacy of medicinal plant extracts against Anopheles stephensi and Culex quinquefasciatus (Diptera: Culicidae). *Trop. Biomed.* **2010**, *27*, 211−219.

(10) Chandran, S. P.; Chaudhary, M.; Pasricha, R.; Ahmad, A.; Sastry, M. Synthesis of gold nanotriangles and silver nanoparticles using Aloe vera plant extract. *Biotechnol. Prog.* **2006**, *22*, 577−583.

(11) Ledwith, D. M.; Whelan, A. M.; Kelly, J. M. A rapid, straightforward method for controlling the morphology of stable silver nanoparticles. *J. Mater. Chem.* **2007**, *17*, 2459.

(12) Brichkin, S. B.; Spirin, M. G.; Nikolenko, L. M.; Nikolenko, D. Y.; Gak, V. Y.; Ivanchikhina, A. V.; Razumov, V. F. The use of reversed micelles for the synthesis of nanoparticles. *High Energy Chem.* **2008**, *42*, 516−521.

(13) Malynych, S. Z.; Chumanov, G. Vacuum deposition of silver island films on chemically modified surfaces. *J. Vac. Sci. Technol., A* **2003**, *21*, 723−727.

(14) Patil, C. D.; Patil, S. V.; Borase, H. P.; Salunke, B. K.; Salunkhe, R. B. Larvicidal activity of silver nanoparticles synthesized using Plumeria rubra plant latex against Aedes aegypti and Aedes stephensi. *Parasitol. Res.* **2012**, *110*, 1815−1822.

(15) Mangalampalli, B.; Dumala, N.; Grover, P. Acute oral toxicity study of magnesium oxide nanoparticles and microparticles in female albino Wistar rats. *Regul. Toxicol. Pharmacol.* **2017**, *90*, 170−184.

(16) Sierra-Fernandez, A. S.; De la Rosa-García, S. C. D. L. R.; Gomez-Villalba, L. S. G.; Gómez-Cornelio, S. G.; Rabanal, M. E.; Fort, R.; Quintana, P. Synthesis, Photocatalytic, and Antifungal Properties of MgO, ZnO and Zn/Mg Oxide Nanoparticles for the Protection of Calcareous Stone Heritage. *ACS Appl. Mater. Interfaces* **2017**, *9*, 24873−24886.

(17) Krishnamoorthy, K.; Moon, J. Y.; Hyun, H. B.; Cho, S. K.; Kim, S. J. Mechanistic investigation on the toxicity of MgO nanoparticles toward cancer cells. *J. Mater. Chem.* **2012**, *22*, 24610−24617.

(18) Naeimi, H.; Alishahi, N. Nanocrystalline magnesium oxide as solid base catalyst in the presence of iodine promoted one-pot synthesis of 2-substituted benzimidazole derivatives under mild conditions. *J. Exp. Nanosci.* **2015**, *10*, 222−234.

(19) Makhluf, S.; Dror, R.; Nitzan, Y.; Abramovich, Y.; Jelinek, R.; Gedanken, A. Microwave-Assisted Synthesis of Nanocrystalline MgO and Its Use as a Bacteriocide. *Adv. Funct. Mater.* **2005**, *15*, 1708−1715.

(20) Yuvarajan, R.; Natarajan, D.; Jayavel, R. Green synthesized silver nanoparticles from indoneesiella echioides and its antibacterial potential. *Indo Am. J. Pharm. Res.* **2014**, *4*, 5121−5128.

(21) Mazaheri, N.; naghsh, N.; Karimi, A.; Salavati, H. *In vivo* Toxicity Investigation of Magnesium Oxide Nanoparticles in Rat for Environmental and Biomedical Applications. *Iran. J. Biotechnol.* **2019**, *17*, 1.

(22) Younis, I. Y.; El-Hawary, S. S.; Eldahshan, O. A.; et al. Green synthesis of magnesium nanoparticles mediated from *Rosa floribunda* charisma extract and its antioxidant, antiaging and antibiofilm activities. *Sci. Rep.* **2021**, *11*, 16868.

(23) Ashok, C.; Rao, K. V.; Chakra, C. S.; Rao, K. G. MgO Nanoparticles Prepared By Microwave-Irradiation Technique and Its Seed Germination Application. *NanoTrends J. Nanotechnol. Appl.* **2016**, *18*, 10.

(24) Pudukudy, M.; Yaakob, Z.; Mazuki, M. Z.; Takriff, M. S.; Jahaya, S. S. One-pot sol-gel synthesis of MgO nanoparticles supported nickel and iron catalysts for undiluted methane decomposition into COx free hydrogen and nanocarbon. *Appl. Catal., B* **2017**, *218*, 298−316.

(25) World Health Organization. *Report of the WHO informal consultation on the evaluation on the testing of insecticides*. CTD/WHO PES/IC/96.1; WHO: Geneva, 1996; Vol. *69*.

(26) Rahuman, A. A.; Gopalakrishnan, G.; Ghouse, B. S.; Arumugam, S.; Himalayan, B. Effect of Feronia limonia on mosquito larvae. *Fitoterapia* **2000**, *71*, 553−555.

(27) Idowu, E. T.; Adeogun, A. O.; Adams, L. A.; et al. Larvicidal potential of two silver nano-particles (Moringa oleifera and Ficus exasperata) against laboratory and field strains of Anopheles gambiae (Diptera: Culicidae) in Lagos, Nigeria. *JOBAZ* **2021**, *82*, 7.

(28) Saied, E.; Eid, A. M.; Hassan, S. E.; Salem, S. S.; Radwan, A. A.; Halawa, M.; Saleh, F. M.; Saad, H. A.; Saied, E. M.; Fouda, A. The Catalytic Activity of Biosynthesized Magnesium Oxide Nanoparticles (MgO-NPs) for Inhibiting the Growth of Pathogenic Microbes, Tanning Effluent Treatment, and Chromium Ion Removal. *Catalysts* **2021**, *11*, 821.

(29) Abdallah, Y.; Ogunyemi, S. O.; Abdelazez, A.; Zhang, M.; Hong, X.; Ibrahim, E.; Hossain, A.; Fouad, H.; Li, B.; Chen, J. The Green Synthesis of MgO Nano-Flowers Using *Rosmarinus officinalis* L. (Rosemary) and the Antibacterial Activities against *Xanthomonas oryzae* pv. Oryzae. *BioMed Res. Int.* **2019**, *2019*, 5620989.

(30) Imani, M. M.; Safaei, M. Optimized Synthesis of Magnesium Oxide Nanoparticles as Bactericidal Agents. *J. Nanotechnol.* **2019**, *2019*, 6063832.

(31) Rahmani-Nezhad, S.; Dianat, Sh.; Saeedi, M.; Hadjiakhoondi, A. Synthesis Characterization and Catalytic Activity of Plant-Mediated MgO nanostructures Using Mucuna Pruriens L. Seed Extract and Their Biological Evaluation. *J. nanoanalysis* **2017**, *4*, 290.

(32) Amina, M. N. M. A.; Al Musayeib, M. F. E.; Alarfaj, H. F.; El-Tohamy, G. A. A.; Oraby, S. I.; Al Hamoud, N. M. S.; Bukhari, S. I.; Moubayed, N. M. S. Biogenic green synthesis of MgO nanoparticles using Saussurea costus biomasses for a comprehensive detection of their antimicrobial, cytotoxicity against MCF-7 breast cancer cells and photocatalysis potentials. *PLoS One* **2020**, *15*, No. e0237567.
(33) Dobrucka, R. Synthesis of MgO Nanoparticles Using *Artemisia abrotanum* Herba Extract and Their Antioxidant and Photocatalytic Properties. *Iran. J. Sci. Technol. Trans. A-Science* **2018**, *42*, 547−555.
(34) Suresh, J.; Pradheesh, G.; Alexramani, V.; Sundrarajan, M.; Hong, S. I. Green synthesis and characterization of hexagonal shaped MgO nanoparticles using insulin plant (Costus pictus D. Don) leave extract and its antimicrobial as well as anticancer activity. *Adv. Powder Technol.* **2018**, *29*, 1685−1694.
(35) Hassan, S. E. D.; Fouda, A.; Saied, E.; Farag, M.; Eid, A. M.; Barghoth, M. G.; Awad, M. A.; Hamza, M. F.; Awad, M. F. Rhizopus Oryzae-mediated green synthesis of magnesium oxide nanoparticles (MgO-NPs): A promising tool for antimicrobial, mosquitocidal action, and tanning effluent treatment. *J. Fungi* **2021**, *7*, 372.
(36) Huang, L.; Li, D. Q.; Lin, Y. J.; Wei, M.; Evans, D. G.; Duan, X. Controllable preparation of Nano-MgO and investigation of its bactericidal properties. *J. Inorg. Biochem.* **2005**, *99*, 986−993.
(37) Nel, A.; Xia, T.; Mädler, L.; Li, N. Toxic Potential of Materials at the Nanolevel. *Science* **2006**, *311*, 622−627.
(38) Pal, S.; Tak, Y. K.; Song, J. M. Does the Antibacterial Activity of Silver Nanoparticles Depend on the Shape of the Nanoparticle? A Study of the Gram-Negative Bacterium Escherichia coli. *Appl. Environ. Microbiol.* **2007**, *73*, 1712−1720.
(39) Jin, T.; He, Y. Antibacterial activities of magnesium oxide (MgO) nanoparticles against foodborne pathogens. *J. Nanopart. Res.* **2011**, *13*, 6877−6885.
(40) Emamifar, A.; Kadivar, M.; Shahedi, M.; Soleimanian-Zad, S. Effect of nanocomposite packaging containing Ag and ZnO on inactivation of Lactobacillus plantarum in orange juice. *Food Control* **2011**, *22*, 408−413.
(41) Kim, J. S.; Kuk, E.; Yu, K. N.; Kim, J. H.; Park, S. J.; Lee, H. J.; Kim, S. H.; Park, Y. K.; Park, Y. H.; Hwang, C. Y.; Kim, Y. K.; Lee, Y. S.; Jeong, D. H.; Cho, M. H. Antimicrobial effects of silver nanoparticles. *Nanomedicine* **2007**, *3*, 95−101.
(42) Lin, Y. J.; Xu, X. Y.; Huang, L.; Evans, D. G.; Li, D. Q. Bactericidal properties of ZnO−Al2O3 composites formed from layered double hydroxide precursors. *J. Mater. Sci.: Mater. Med.* **2009**, *20*, 591−595.
(43) Yamamoto, O.; Ohira, T.; Alvarez, K.; Fukuda, M. Antibacterial characteristics of CaCO3−MgO composites. *Mater. Sci. Eng. B* **2010**, *173*, 208−212.
(44) Yamamoto, O.; Fukuda, T.; Kimata, M.; Sawai, J.; Sasamoto, T. Antibacterial characteristics of MgO-mounted spherical carbons prepared by carbonization of ion-exchanged resin. *J. Ceram. Soc. Jpn.* **2001**, *109*, 363−365.
(45) Senthil, B.; Rajasekar, A.; Devasena, T. Mechanism of Bactericidal Action of Biosynthesized Silver Nanoparticles. *Res. J. Biotechnol.* **2018**, *13*, 72−78.
(46) Suresh, M.; Jeevanandam, J.; Chan, Y. S.; Danquah, M. K.; Kalaiarasi, J. M. V. Opportunities for metal oxide nanoparticles as a potential mosquitocide. *Bionanoscience* **2020**, *10*, 292.
(47) Mouchet, F.; Landois, P.; Sarremejean, E.; Bernard, G.; Puech, P.; Pinelli, E.; Flahaut, E.; Gauthier, L. Characterisation and in vivo ecotoxicity evaluation of double-wall carbon nanotubes in larvae of the amphibian Xenopus laevis. *Aquat. Toxicol.* **2008**, *87*, 127−137.
(48) Podder, S.; Chanda, D.; Mukhopadhyay, A. K.; De, A.; Das, B.; Samanta, A.; Hardy, J. G.; Ghosh, C. K. Effect of Morphology and Concentration on Crossover between Antioxidant and Pro-oxidant Activity of MgO Nanostructures. *Inorg. Chem.* **2018**, *57*, 12727−12739.
(49) Jayaseelan, C.; Rahuman, A. A.; Rajakumar, G.; Vishnu Kirthi, A.; Santhoshkumar, T.; Marimuthu, S.; Bagavan, A.; Kamaraj, C.; Zahir, A. A.; Elango, G. Synthesis of pediculocidal and larvicidal silver nanoparticles by leaf extract from heartleaf moonseed plant, Tinospora cordifolia Miers. *Parasitol. Res.* **2011**, *109*, 185−194.
(50) Santhoshkumar, T.; Rahuman, A. A.; Rajakumar, G.; Marimuthu, S.; Bagavan, A.; Jayaseelan, C.; Zahir, A. A.; Elango, G.; Kamaraj, C. Synthesis of silver nanoparticles using Nelumbo nucifera leaf extract and its larvicidal activity against malaria and filariasis vectors. *Parasitol. Res.* **2011**, *108*, 693−702.
(51) Karthik, K.; Dhanuskodi, S.; Gobinath, C.; Prabukumar, S.; Sivaramakrishnan, S. Fabrication of MgO nanostructures and its efficient photocatalytic, antibacterial and anticancer performance. *J. Photochem. Photobiol., B* **2019**, *190*, 8−20.
(52) Leung, Y. H.; Xu, X.; Ma, A. P.; Liu, F.; Ng, A.; Shen, Z.; Gethings, L. A.; Guo, M. Y.; Djurišić, A. B.; Lee, P. K.; Lee, H. K.; Chan, W. K.; Leung, F. C. C. Toxicity of ZnO and TiO2 to Escherichia coli cells. *Sci. Rep.* **2016**, *6*, 1−13.
(53) Magdolenova, Z.; Collins, A.; Kumar, A.; Dhawan, A.; Stone, V.; Dusinska, M. Mechanisms of genotoxicity. A review of in vitro and in vivo studies with engineered nanoparticles. *Nanotoxicology* **2014**, *8*, 233−278.
(54) Pugazhendhi, A.; Prabhu, R.; Muruganantham, K.; Shanmuganathan, R.; Natarajan, S. Anticancer, antimicrobial and photocatalytic activities of green synthesized magnesium oxide nanoparticles (MgONPs) using aqueous extract of Sargassum wightii. *J. Photochem. Photobiol., B* **2019**, *190*, 86−97.

https://doi.org/10.1021/acsomega.2c01450
ACS Omega 2023, 8, 5225−5233